

# Probing top-quark flavor-changing couplings at the CEPC

Liaoshan Shi (石辽珊)<sup>1</sup> Cen Zhang (张岑)<sup>1,2</sup>

<sup>1</sup> Institute of High Energy Physics, Chinese Academy of Sciences, Beijing 100049, China

<sup>2</sup> School of Physical Sciences, University of Chinese Academy of Sciences, Beijing 100049, China

**Abstract:** We propose to study the flavor properties of the top quark at the future Circular Electron Positron Collider (CEPC) in China. We systematically consider the full set of 56 real parameters that characterize the flavor-changing neutral interactions of the top quark, which can be tested at the CEPC by the single top production channel. Compared with current bounds from the LEP2 data and the projected limits at the high-luminosity LHC, we find that the CEPC could improve the limits on four-fermion flavor-changing coefficients by one to two orders of magnitude, and in the meantime providing similar sensitivities on two-fermion flavor-changing coefficients. Overall, the CEPC could explore a large fraction of currently allowed parameter space that will not be covered by the upgrade of the LHC. We show that the  $c$ -jet tagging capacity at the CEPC could further improve its sensitivity to top-charm flavor-changing couplings. If a signal is observed, the kinematic distribution as well as the  $c$ -jet tagging could be exploited to pinpoint the sizes of various flavor-changing couplings, providing valuable information on the flavor properties of the top quark.

**Key words:** top quark, flavor-changing neutral current, lepton collider

**PACS:** 13.66.Bc, 14.65.Ha, 14.80.Bn

## 1 Introduction

After the discovery of the Higgs boson [1, 2], the focus of high energy physics is to study its properties in detail. While the Higgs measurements at the Large Hadron Collider (LHC) will finally reach a precision level of about 5%~10% (except for the Higgs trilinear coupling), precision measurements of Higgs couplings could further benefit from the cleaner environment of a future  $e^+e^-$  collider. Among several proposals, the Circular Electron Positron Collider (CEPC) in China [3, 4] is proposed to run as a Higgs factory with collisions at 240 GeV, which maximizes the  $e^+e^- \rightarrow HZ$  cross section, producing at least a million Higgs bosons over a period of 7 years.

Apart from the Higgs boson, the top quark could play an equally important role in the electroweak symmetry breaking mechanism. By virtue of its large mass, it is often thought of as a window to new physics. Producing top-quark pairs at a lepton collider would however require a minimum center of mass energy of about  $2m_t \approx 345$  GeV, beyond the currently planned energy of the CEPC. While an energy upgrade above the  $t\bar{t}$  threshold remains an open option, an interesting question to ask is whether we could still learn something about the top quark at an energy below the production threshold. One possibility, for instance, is to study instead the virtual top quarks, which appear in almost all electroweak processes due to quantum corrections [5–7].

In this work, we study a different possibility: in-

stead of producing pairs of top quarks on shell, single top quark can be produced in association with a light quark. The process  $e^+e^- \rightarrow t(\bar{t})j$  is possible with  $E_{cm} = 240$  GeV. This process is highly suppressed by the Glashow-Iliopoulos-Maiani (GIM) mechanism [8] in the Standard Model (SM), but if physics beyond the SM exists and gives rise to the so called top-quark flavor-changing neutral (FCN) interactions, this production mode could happen via an  $s$ -channel  $Z$  or photon, or via a contact four-fermion FCN interaction. The top-quark FCN couplings have been searched for at the LHC, the Tevatron, the LEP2 and the HERA experiments [9–50]. Currently, the best constraints on two-fermion FCN couplings are coming from the LHC, while the four-fermion contact interactions have received much less attention, even though the latter is indispensable for a complete description of FCN couplings and is also motivated by studying explicit models beyond the SM [51–54]. Interestingly, it has been shown that so far the best sensitivity on these contact interactions is still dominated by the LEP2 experiment, despite its much lower integrated luminosity [51, 55]. The LHC and LEP2 thus provide complementary constraints in the theory space spanned by the two types of FCN interactions. This immediately implies that a future  $e^+e^-$  collider will further improve our knowledge of the top-quark flavor properties. The goal of this paper is to study the CEPC prospects on top FCN couplings, to demonstrate that a similar complementarity is expected

<sup>1</sup> E-mail: liaoshan.shi@cern.ch

<sup>2</sup> E-mail: cenzhang@ihep.ac.cn

between the CEPC and high-luminosity LHC (HL-LHC) prospects, and to provide inputs for the CEPC experiment. Similar prospects have been provided previously for TESLA, FCC-ee, and CLIC [56–58], but only the CLIC report [58] has considered four-fermion interactions.

The paper is organized as follows. In Section 2 we describe the theory background, with a focus on the two-fermion FCN and four-fermion FCN interactions, and their different sensitivities at a hadron collider and a  $e^+e^-$  collider. In Section 3 we give the details of our simulation and our analysis strategy. In Section 4 we show our results and discuss possible improvements. Section 5 is our conclusion. Some additional results can be found in Appendix A.

## 2 Flavor changing effective operators

FCN interaction of the top quark is highly suppressed by the GIM mechanism. Branching ratios for two-body top FCN decays in the SM are at the orders of  $10^{-12}$ – $10^{-15}$  [59–61]. Any hint for such processes would thus immediately point to physics beyond the SM. A wide variety of limits have been set on these couplings. For example, flavor changing decay modes  $t \rightarrow qZ$  and  $t \rightarrow q\gamma$  have been searched for at the Tevatron by CDF [9–11] and D0 [12], and at the LHC by ATLAS [13–17] and CMS [18–20]. At the LHC  $t \rightarrow qH$  has also been searched for [21–30]. Direct top production,  $pp \rightarrow t$ , has been considered at the Tevatron by CDF [31] and at the LHC by ATLAS [32–34], while a similar production with an additional jet in the final state has been considered by D0 [35, 36] and CMS [37]. Single top production in association with a photon and a  $Z$  have been searched by CMS [38] and ATLAS [39]. At LEP2,  $e^+e^- \rightarrow tj$  has been investigated by all four collaborations [40–45], while at HERA, the single-top  $e^-p \rightarrow e^-t$  production has been considered by ZEUS [46, 47] and H1 [48–50]. The most constraining limits have been recently collected and summarized in Table 33 of Ref. [55]. The sensitivities in terms of two-body branching ratios are roughly at order  $10^{-4}$  to  $10^{-3}$ , approaching the expected sizes from typical new physics models [62].

A complete and systematic description of top-quark FCN couplings based on the Standard Model Effective Field Theory (SMEFT) [63–65] has been discussed and documented in the LHC TOP Working Group note [66]. The idea is that starting from the Warsaw basis operators [67], one defines the linear combinations of Wilson coefficients that give independent contributions in a given measurement. For the  $e^+e^- \rightarrow tj$  process, the relevant basis operators are the following two-fermion operators

$$O_{\varphi q}^{1(ij)} = (\varphi^\dagger i\overleftrightarrow{D}_{\mu\varphi}) (\bar{q}_i \gamma^\mu q_j), \quad (1)$$

$$O_{\varphi q}^{3(ij)} = (\varphi^\dagger i\overleftrightarrow{D}_{\mu\varphi}^I) (\bar{q}_i \gamma^\mu \tau^I q_j), \quad (2)$$

$$O_{\varphi u}^{(ij)} = (\varphi^\dagger i\overleftrightarrow{D}_{\mu\varphi}) (\bar{u}_i \gamma^\mu u_j), \quad (3)$$

$$O_{uW}^{(ij)} = (\bar{q}_i \sigma^{\mu\nu} \tau^I u_j) \tilde{H} W_{\mu\nu}^I, \quad (4)$$

$$O_{uB}^{(ij)} = (\bar{q}_i \sigma^{\mu\nu} u_j) \tilde{H} B_{\mu\nu}, \quad (5)$$

and the following four-fermion operators

$$O_{lq}^{1(ijkl)} = (\bar{l}_i \gamma_\mu l_j) (\bar{q}_k \gamma^\mu q_l), \quad (6)$$

$$O_{lq}^{3(ijkl)} = (\bar{l}_i \gamma_\mu \tau^I l_j) (\bar{q}_k \gamma^\mu \tau^I q_l), \quad (7)$$

$$O_{lu}^{(ijkl)} = (\bar{l}_i \gamma_\mu l_j) (\bar{u}_k \gamma^\mu u_l), \quad (8)$$

$$O_{eq}^{(ijkl)} = (\bar{e}_i \gamma_\mu e_j) (\bar{q}_k \gamma^\mu q_l), \quad (9)$$

$$O_{eu}^{(ijkl)} = (\bar{e}_i \gamma_\mu e_j) (\bar{u}_k \gamma^\mu u_l), \quad (10)$$

$$O_{lequ}^{1(ijkl)} = (\bar{l}_i e_j) \varepsilon (\bar{q}_k u_l), \quad (11)$$

$$O_{lequ}^{3(ijkl)} = (\bar{l}_i \sigma_{\mu\nu} e_j) \varepsilon (\bar{q}_k \sigma^{\mu\nu} u_l), \quad (12)$$

where  $i, j, k, l$  are flavor indices. Other operators such as  $O_{u\varphi}^{(ij)}$  and  $O_{uG}^{(ij)}$  could lead to FCN couplings  $tqH$  and  $tqg$ , but they cannot be probed in the single top channel. The following linear combinations of Wilson coefficients can be defined as the independent degrees of freedom that enter this process:

Two-fermion degrees of freedom:

$$c_{\varphi q}^{-[I](3+a)} \equiv \frac{[\mathfrak{S}]}{\mathfrak{R}} \{ C_{\varphi q}^{1(3a)} - C_{\varphi q}^{3(3a)} \}, \quad (13)$$

$$c_{\varphi u}^{[I](3+a)} \equiv \frac{[\mathfrak{S}]}{\mathfrak{R}} \{ C_{\varphi u}^{1(3a)} \}, \quad (14)$$

$$c_{uA}^{[I](3a)} \equiv \{ c_W C_{uB}^{(3a)} + s_W C_{uW}^{(3a)} \}, \quad (15)$$

$$c_{uA}^{[I](a3)} \equiv \{ c_W C_{uB}^{(a3)} + s_W C_{uW}^{(a3)} \}, \quad (16)$$

$$c_{uZ}^{[I](3a)} \equiv \{ -s_W C_{uB}^{(3a)} + c_W C_{uW}^{(3a)} \}, \quad (17)$$

$$c_{uZ}^{[I](a3)} \equiv \{ -s_W C_{uB}^{(a3)} + c_W C_{uW}^{(a3)} \}. \quad (18)$$

Four-fermion degrees of freedom:

$$c_{lq}^{-[I](1,3+a)} \equiv \frac{[\mathfrak{S}]}{\mathfrak{R}} \{ C_{lq}^{1(113a)} - C_{lq}^{3(113a)} \}, \quad (19)$$

$$c_{eq}^{[I](1,3+a)} \equiv \frac{[\mathfrak{S}]}{\mathfrak{R}} \{ C_{eq}^{(113a)} \}, \quad (20)$$

$$c_{lu}^{[I](1,3+a)} \equiv \frac{[\mathfrak{S}]}{\mathfrak{R}} \{ C_{lu}^{(113a)} \}, \quad (21)$$

$$c_{eu}^{[I](1,3+a)} \equiv \frac{[\mathfrak{S}]}{\mathfrak{R}} \{ C_{eu}^{(113a)} \}, \quad (22)$$

$$c_{lequ}^{S[I](1,3a)} \equiv \frac{[\mathfrak{S}]}{\mathfrak{R}} \{ C_{lequ}^{1(113a)} \}, \quad (23)$$

$$c_{lequ}^{S[I](1,a3)} \equiv \frac{[\mathfrak{S}]}{\mathfrak{R}} \{ C_{lequ}^{1(11a3)} \}, \quad (24)$$

$$c_{lequ}^{T[I](1,3a)} \equiv \frac{[\mathfrak{S}]}{\mathfrak{R}} \{ C_{lequ}^{3(113a)} \}, \quad (25)$$

$$c_{lequ}^{T[I](1,a3)} \equiv \frac{[\mathfrak{S}]}{\mathfrak{R}} \{ C_{lequ}^{3(11a3)} \}, \quad (26)$$

where quark generation indices ( $a = 1, 2$ ) and lepton generation indices are enclosed in parentheses. An  $I$  in the

superscript represents the imaginary part of the coefficient. In total, one collects the following 28 real and

independent degrees of freedom for each  $a$  (and thus 56 in total):

$$\begin{array}{cccccccc}
 c_{\varphi q}^{-(3+a)} & c_{uZ}^{(a3)} & c_{uA}^{(a3)} & c_{lq}^{-(1,3+a)} & c_{eq}^{(1,3+a)} & c_{lequ}^{S(1,a3)} & c_{lequ}^{T(1,a3)} \\
 c_{\varphi u}^{(3+a)} & c_{uZ}^{(3a)} & c_{uA}^{(3a)} & c_{lu}^{(1,3+a)} & c_{eu}^{(1,3+a)} & c_{lequ}^{S(1,3a)} & c_{lequ}^{T(1,3a)} \\
 c_{\varphi q}^{-I(3+a)} & c_{uZ}^{I(a3)} & c_{uA}^{I(a3)} & c_{lq}^{-I(1,3+a)} & c_{eq}^{I(1,3+a)} & c_{lequ}^{SI(1,a3)} & c_{lequ}^{TI(1,a3)} \\
 c_{\varphi u}^{I(3+a)} & c_{uZ}^{I(3a)} & c_{uA}^{I(3a)} & c_{lu}^{I(1,3+a)} & c_{eu}^{I(1,3+a)} & c_{lequ}^{SI(1,3a)} & c_{lequ}^{TI(1,3a)}
 \end{array} \tag{27}$$

Among the seven columns, the first three come from two-fermion operators. The  $c_{\varphi q}^-$  and  $c_{\varphi u}$  give rise to  $tqZ$  coupling with a vector-like Lorentz structure, while  $c_{uA}$  and  $c_{uZ}$  give rise to the  $tq\gamma$  and  $tqZ$  dipole interactions. The last four come from  $tqee$  four-fermion operators.  $c_{lq}^-$ ,  $c_{lu}$ ,  $c_{eq}$ , and  $c_{eu}$  coefficients give rise to interactions between two vector currents, while  $c_{lequ}^S$  and  $c_{lequ}^T$  to interactions between two scalar and two tensor currents, respectively. We note that the first two rows are CP-even while the last two rows are CP-odd. The first and the third rows involve a left-handed light quark while the second and the fourth rows involve a right-handed light quark. The interference between coefficients from different rows in the limit of massless quarks vanishes for this reason. Furthermore, the signatures of the degrees of freedom in the first row are identical to the ones from the third row, and similarly the second row identical to the fourth row. This is because of the absence of SM amplitude to interfere with the FCN coefficients, which leads to cross sections that are invariant under a change of phase:  $c_i + c_i^I i \rightarrow e^{i\delta} (c_i + c_i^I i)$ . It is therefore sufficient to focus on the degrees of freedom in the first two rows, and in the rest of the paper we will refer to them simply as coefficients. We also note that the  $e^+e^- \rightarrow tj$  signal of the coefficients from the first two rows are similar, up to a  $\theta \rightarrow \pi - \theta$  transformation in the scattering angle of the  $tj$  production. The decay of the top quark however breaks this similarity. This is because the two coefficients produce left-handed and right-handed top quarks respectively, while the lepton momentum from the top decay is correlated with the top helicity. This leads to difference in signal efficiencies between the first two rows.

Two-fermion FCN interactions in the first three columns are considered in almost all experimental searches. Four-fermion FCN interactions, on the other hand, have unduly been neglected. They have been proposed by Ref. [68], and later searched at the LEP2 by the L3 and DELPHI collaborations [43, 45], but the three-body decay through four-fermion FCN interactions have never been searched at Tevatron or LHC. For prospects on future  $e^+e^-$  colliders, four-fermion couplings have also been neglected in the studies of single top at TESLA and

at FCC-ee [56, 57], though the recent CLIC yellow report has included them [58]. However, four-fermion operators are indispensable for a complete characterization of the top-quark flavor properties. They could arise, for example, in the presence of a heavy mediator coupling to one top quark and one light quark, or in cases where equation of motion (EOM) is used to remove redundant two-fermion operators in terms of the basis operators. Their existence also guarantees the correctness of the effective description when particles go off-shell or in loops, see [51] for a detailed discussion. The three-body decay  $t \rightarrow cf\bar{f}$  have been calculated in several explicit models [52–54], giving further motivations for the consideration of  $tcll$  contact operators. Ref. [69] has recast the LHC constraints on  $t \rightarrow qZ$  to provide bounds. Finally, the lepton-and-quark-flavor violating top decay through contact interactions has been studied in [70], and recently searched by the ATLAS collaboration [71].

An interesting fact about the four-fermion FCN interaction is that the most stringent limits so far are still coming from the LEP2 experiments. In Ref. [55], a global analysis based on the current bounds have been performed within the SMEFT framework. The result clearly shows that the LHC is more sensitive to the two-fermion operator coefficients, while the LEP2 is more sensitive to the four-fermion ones. As a result, currently their results are complementary to each other in the full parameter space, as demonstrated in Figure 59 in Section 8.1 of Ref. [55]. The complementarity persists even with the HL-LHC (see Figure 59 right of Ref. [55]), despite the orders of magnitude difference between the LEP2 and HL-LHC luminosities. Clearly, this implies that an  $e^+e^-$  collider with higher luminosity will continue to provide valuable information about top FCN interactions, and explore the parameter space which will be left uncovered at the HL-LHC.

The difference in sensitivities between the two types of machines can be understood as follows. The two-fermion operators can be searched, at the LHC, by the flavor-changing decays of the top quark, but the same decay through a four-fermion operator is a three-body one, and will be suppressed by additional phase space

factor. For illustration, the decay rates of  $t \rightarrow ce^+e^-$  through  $c_{\varphi u}$ ,  $c_{uZ}$  and  $c_{eu}$  are  $8.1 \times 10^{-5}$ ,  $2.4 \times 10^{-4}$  GeV and  $3.2 \times 10^{-6}$  GeV respectively, for  $c/\Lambda^2 = 1$  TeV $^{-2}$ . Furthermore, the  $e^+e^-$  mass spectrum is a continuum one, and thus the best sensitivity requires a dedicated search without using a mass window cut (see discussions in Refs. [51, 69]). Searching for four-fermion operators in single top channels at a hadron collider would suffer from the same phase-space suppression. The situation in an  $e^+e^-$  collider is however different. Two-fermion operators can be searched for through single top  $e^+e^- \rightarrow Z^*/\gamma^* \rightarrow tj$  (or through top decay if the center of mass energy allows for top-quark pair production, though typically the former has a better sensitivity [56]). Going to four-fermion operator case, instead of a suppression effect, the production rate is actually enhanced due to one less propagator than the two-fermion cases. For illustration, the single top production cross section at  $E_{cm} = 240$  GeV for  $c_{\varphi u}$ ,  $c_{uZ}$  and  $c_{eu}$  are 0.0018 pb, 0.020 pb and 0.12 pb respectively, for  $c/\Lambda^2 = 1$  TeV $^{-2}$ , and this enhancement effect increases with energy. The comparison of the two cases is illustrated in Figure 1.

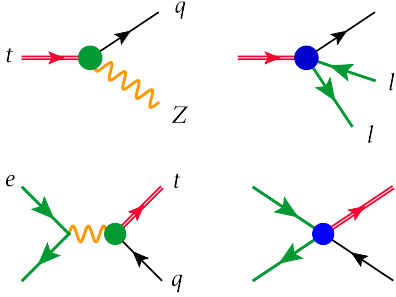


Fig. 1. Top: flavor-changing decay at the LHC. The four-fermion operator contribution is suppressed by additional phase space factor compared with the two-fermion contribution. Bottom: flavor-changing single top at a  $e^+e^-$  collider. The four-fermion operator contribution is enhanced due to one less  $s$ -channel propagator than the two-fermion case. Green and blue dots represent two- and four-fermion operator insertions.

### 3 Simulation

To study the prospects on top FCN couplings, we consider the scenario of CEPC running with a center of mass energy  $E_{cm} = 240$  GeV and an integrated luminosity of  $5.6 \text{ ab}^{-1}$ . We simulate the signal and background at leading order with parton shower, by using MADGRAPH5\_AMC@NLO [72] and PYTHIA8 [73, 74]. The signal is generated with the UFO model [75, 76], DIM6TOP, which follows the LHC TopWG EFT recommendation [66] and is available at [https://feynrules.](https://feynrules.irmp.ucl.ac.be/wiki/dim6top)

[irmp.ucl.ac.be/wiki/dim6top](https://feynrules.irmp.ucl.ac.be/wiki/dim6top). Detector level simulation is performed with DELPHES with the default CEPC card [77]. Jets are reconstructed using the FASTJET package [78] with the anti- $k_t$  algorithm [79] with a radius parameter of 0.5. Automatic calculation for QCD corrections to processes involving only two-fermion FCN operators have been developed in Ref. [80] (see also Refs. [81–89] where results for other top flavor-changing channels have been presented). The corresponding  $K$ -factors for the signal are around 1.2, which corresponds to roughly 10% change in the coefficients. We expect the corrections to four-fermion operators to be at the same level, and therefore neglect these corrections in this work. The dominant background comes from  $W$ -pair and  $Z$ -pair production, and we do not expect a significant change at next-to-leading order in QCD.

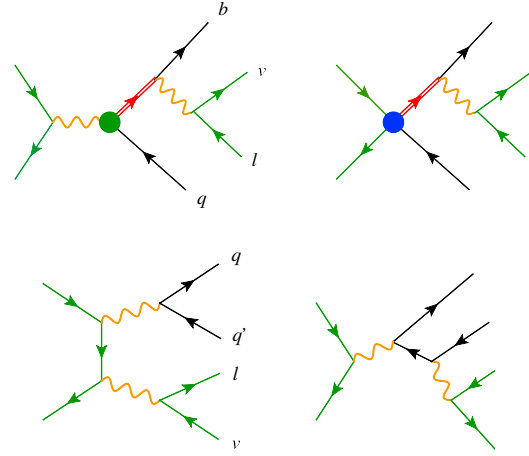


Fig. 2. Selected Feynman diagrams for signal (top) and background (bottom). Green and blue dots represent two- and four-fermion operator insertions. Red double lines represent top-quark propagators.

We consider the top-quark decaying semi-leptonically. The signal final state is  $bjl\nu$ , where  $j$  is an up or charm quark jet. The dominant background is  $qq'l\nu$ , with one light or charm quark jet misidentified as a  $b$ -jet. A large fraction comes from  $W$  pair production with one  $W$  decaying hadronically and the other leptonically, while diagrams with only one  $W$  resonance could also contribute. Those without any resonances only give negligible contributions [56]. Another source of background is  $qqll$  where the second lepton is missed by the detector. This is included in our simulation, but the contribution is subdominant. Selected diagrams of the signal and the background are shown in Figure 2.

Based on the expected signature of the signal process, we select events with exactly one charged lepton (electron or muon) and at least two jets. The charged lepton must have  $p_T > 10$  GeV and  $|\eta| < 3.0$ . All jets are required to have  $p_T > 20$  GeV and  $|\eta| < 3.0$ . Exactly one

jet should be  $b$ -tagged. If more than one non- $b$ -tagged jets are present, the one with the highest  $p_T$  is selected as the up or charm quark jet candidate. We have chosen a  $b$ -tagging working point with 80% efficiency for  $b$ -jets and a mistagging rate of 10% (0.1%) from  $c$ -jets (light jets) [90]. A missing energy greater than 30 GeV is also required due to the presence of a neutrino. The  $W$  boson candidate is reconstructed from the charged lepton and the missing energy. The top quark candidate is reconstructed by combining the  $W$  boson candidate with the  $b$ -jet.

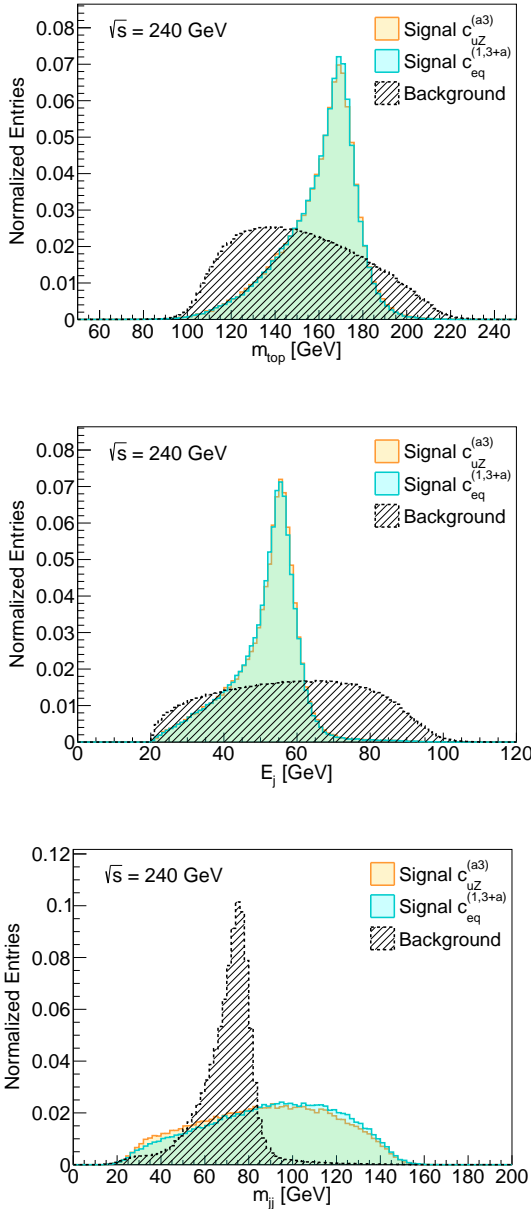


Fig. 3. Signal and background at the reconstruction level. Distributions of  $m_t$ ,  $E_j$ , and  $m_{jj}$  are shown for signals from  $c_{uZ}^{(a3)}$  and  $c_{eq}^{(1,3+a)}$ .

At the parton level, we expect the non- $b$ -tagged jet from the signal to have  $E_j = \frac{s-m_t^2}{2\sqrt{s}} \approx 58$  GeV. For the background, if the contribution comes from diboson production (e.g. Figure 2 down left), we expect the dijet mass to peak at  $m_W = 80.4$  GeV. The contribution from non-resonant diagrams (e.g. Figure 2 down right) however cannot be neglected and gives rise to a continuum spectrum in the dijet mass distribution. At the reconstruction level, it turns out that the energy of the non- $b$ -tagged jet  $E_j$ , the invariant mass of the  $b$ -jet and the non- $b$ -tagged jet  $m_{jj}$ , and the reconstructed top-quark mass  $m_{top}$  are the most useful variables to discriminate the signal from the background. In Figure 3, we plot these variables at the reconstruction level, for the background as well as for the signals from two typical operator coefficients,  $c_{uZ}$  and  $c_{eq}$ , for illustration.

As our baseline analysis, we impose the following kinematic cuts at the reconstruction level

$$E_j < 60 \text{ GeV}, \quad (28)$$

$$m_{jj} > 100 \text{ GeV}, \quad (29)$$

$$m_{top} < 180 \text{ GeV}. \quad (30)$$

These cuts are motivated by Figure 3. The expected number of background events after event selection is about 1400 with an integrated luminosity of  $5.6 \text{ ab}^{-1}$ , corresponding to a statistical uncertainty of about 2.7%. We assume that the systematic uncertainty can be taken under control below this level. The impact of systematic uncertainty can be easily estimated, e.g. a 3% systematic uncertainty will weaken the bound on the cross section by a factor of about 1.5, which corresponds to a factor of 1.2 on the size of coefficients. In the rest of the paper we will simply ignore the systematic effects. We will see that this simple baseline scenario already allows us to obtain reasonable sensitivities. In the next section we will also consider improving it with a template fit.

In the absence of any FCN signal, the 95% confidence level (CL) upper bound on the fiducial cross section is  $0.0134 \text{ fb}$ . Alternatively, the  $5\sigma$  discovery limit on the signal cross section, determined by  $S/\sqrt{B} = 5$ , is a function of the integrated luminosity  $L_{int}$ :

$$\sigma = \frac{5\sqrt{\sigma_B}}{\sqrt{L_{int}}} = \frac{2.51 \text{ fb}}{\sqrt{L_{int}/\text{fb}^{-1}}} \quad (31)$$

The cross section is a quadratic function of the operator coefficients. Including the interference effects, such a function has 28 independent terms for the 7 coefficients in each row of Eq. (27). These terms for the first two rows are the same as those for the last two rows, because they only differ by a CP phase which would never show up in the cross section (without any possible interference with the SM). Thus only 56 independent terms need to be determined for the first two rows for each  $a$ . We sample the parameter space by 56 points and simulate the

fiducial cross section for each of them. The results are fitted to the following form:

$$\sigma = \sum_{a=1,2} \frac{(1 \text{ TeV})^4}{\Lambda^4} \left( \vec{C}_1^a \cdot \mathbf{M}_1^a \cdot \vec{C}_1^{aT} + \vec{C}_2^a \cdot \mathbf{M}_2^a \cdot \vec{C}_2^{aT} \right) \quad (32)$$

where  $\vec{C}_{1,2}$  denote the vectors formed by coefficients in the first and the second rows of Eq. (27).  $a$  is the light quark generation.  $\mathbf{M}_{1,2}^a$  are  $7 \times 7$  matrices. The above result allows us to convert the upper bound and discovery limit on cross section into the 56-dimensional coefficient space.

We have verified the relations between signatures from different rows in Eq. (27): the 1st (2nd) and the 3rd (4th) rows always give the same signatures; the 1st (3rd) and the 2nd (4th) rows at the production level are identical up to a  $\theta \rightarrow \pi - \theta$  transformation in the production angle, but differ if the tops are decayed. In Appendix A, a comparison between the signals from  $c_{uZ}^{(a3)}$ ,  $c_{uZ}^{(3a)}$  and  $c_{uZ}^{J(a3)}$  are shown in Figure 11. A comparison between the signals from  $c_{eq}^{(1,3+a)}$ ,  $c_{eu}^{(1,3+a)}$  and  $c_{eq}^{J(1,3+a)}$  are shown in Figure 12.

## 4 Results

Following our baseline analysis, the 95% CL limits on individual coefficients for the first row are given in Figure 4, where they are compared with the current limits from LHC+LEP2 and with the HL-LHC projection.

FCC-ee projection at the center-of-mass energy of 240 GeV has been given by Ref. [57], but only for the 3 two-fermion coefficients. We show them in the same plot. The CLIC bounds, on the other hand, are only available with higher center-of-mass energy runs and are not shown in the plot. For example, the expected limits on the four-fermion coefficients, from a 380 GeV run for an integrated luminosity of  $500 \text{ fb}^{-1}$ , are about a factor of  $3 \sim 4$  better than those from the CEPC, thanks to the higher beam energy and beam polarization [58].

Looking at the 3 two-fermion coefficients on the left, the limits are either weaker than or comparable to HL-LHC. Still, we emphasize that even in this case the CEPC measurement provides an important consistency check with the existing results. The most interesting result, however, is the improvement on the other four four-fermion coefficients. As expected, we see that they are 1~2 orders of magnitude better than the current limits and the combination of HL-LHC and LEP2. Similar results are observed for the second row operators and are displayed in Figure 13 in Appendix A. In Figure 5 we show the two-dimensional bounds on a two-fermion coefficient  $c_{\varphi q}^{-(3+a)}$  and a four-fermion coefficient  $c_{eq}^{(1,3+a)}$ , compared with LHC, HL-LHC, and LEP2. Clearly, a large fraction of the currently allowed parameter space will be probed by the CEPC. A similar plot for the operators in the second row of Eq. (27) is given in Figure 14 in Appendix A.

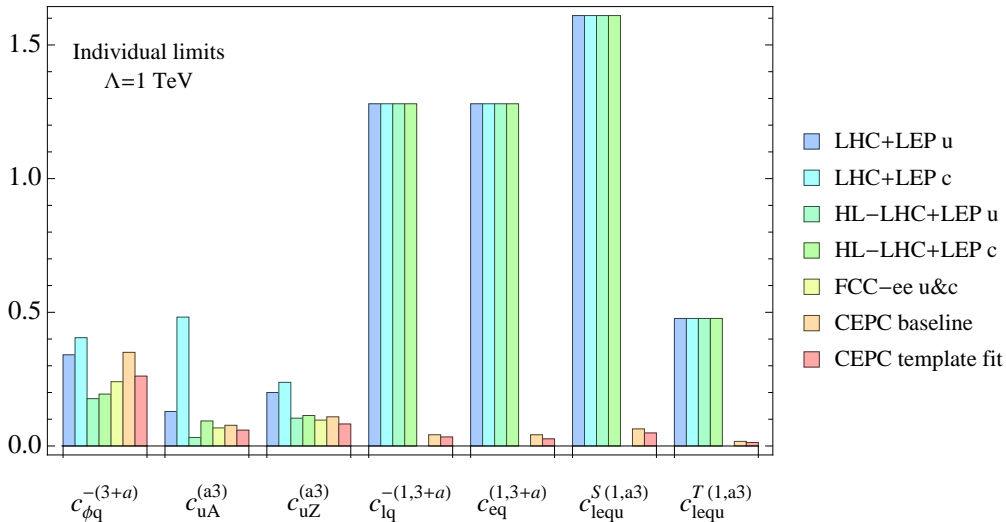


Fig. 4. The 95% CL limits on individual coefficients in the first row of Eq. (27), expected from the CEPC, compared with the existing LHC+LEP2 bounds, and the projected limits from HL-LHC+LEP2 and from FCC-ee with  $3 \text{ ab}^{-1}$  luminosity at 240 GeV (only for the first three coefficients), see Refs. [55, 57]. Results for both generations  $a = 1, 2$  are displayed. The orange column “CEPC baseline” is the expected limits following our baseline analysis, which applies to both flavors ( $a=1,2$ ). The red column “CEPC template fit” uses the  $c$ -jet tagging in its signal definition and only applies to  $a = 2$  operators.

In Figure 6 we plot the discovery limits on the seven coefficients in the first row of Eq. (27), in terms of  $\Lambda/\sqrt{c}$ , as a function of integrated luminosity. This scale is roughly the scale of new physics assuming the coupling is of order one. The plot shows that new physics at a few TeV that leads to four-fermion FCN interactions can be discovered already at quite early stages of the CEPC. The improvement over luminosity is however less significant. Results for the coefficients of the second row are given in the Appendix A, Figure 15.

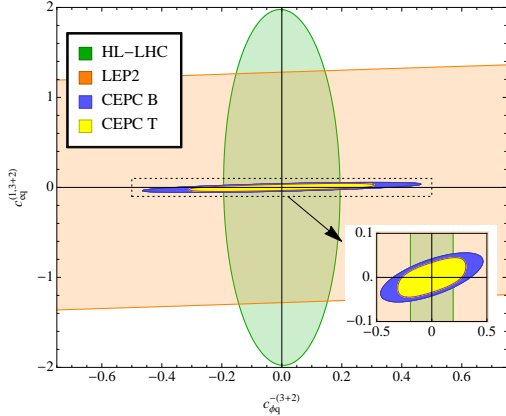


Fig. 5. Two-dimensional bounds on a two-fermion coefficient  $c_{\phi q}^{-(3+2)}$  and a four-fermion coefficient  $c_{e q}^{(1,3+2)}$ , at the 95% CL. Other operators are fixed at 0. The allowed regions from HL-LHC and LEP2 are similar to Figure 59 in Section 8.1 of Ref. [55], except for that there all coefficients are marginalized over. The blue region (“CEPC B”) is the bound expected from the CEPC, following our baseline analysis. The yellow region (“CEPC T”) is obtained with a template fit approach, see more discussions in Section 4.

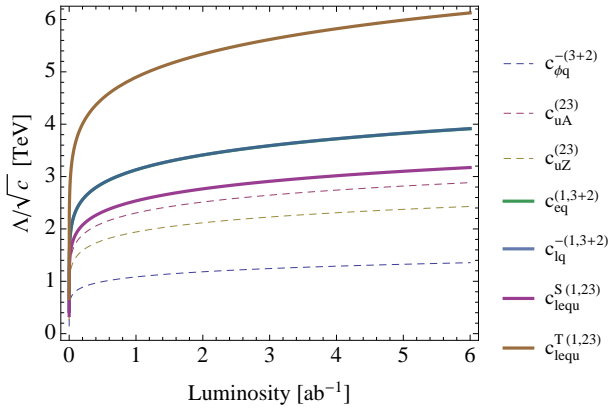


Fig. 6. Five-sigma discovery limit of  $\Lambda/\sqrt{c}$ , which is roughly the scale of new physics, for coefficients in the first row of Eq. (27), as function of integrated luminosity at the CEPC.

Our baseline analysis could be improved by exploiting more features of the signal. One possibility is to make use of heavy flavor tagging. For operators with  $a = 2$ , requiring a tagged  $c$ -jet in the signal definition could largely suppress the background, as most background comes from events with a charm and a strange in the final state, with the charm being mistagged as a  $b$ . The clean environment of CEPC allows for precise determination of displaced vertices and excellent capability of  $c$ -jet tagging [4]. We will assume a working point with 70% tagging efficiency for  $c$ -jets and 20% (12%) mistagging rate from  $b$ -jets (light jets) [90]. To constrain coefficients with  $a = 2$ , we require a  $c$ -jet in the signal definition, while to constrain  $a = 1$  coefficients we veto the events with a  $c$ -jet, though the latter is not expected to significantly change the sensitivity as most background events do not have an extra  $c$ -jet except the one that fakes the  $b$ -jet. Another useful information is the angular distribution of the single top, which is determined by the specific Lorentz structure of the operator. In Figure 7 we show the distributions of the top scattering angle from all 7 coefficients in the first row at the parton level and the reconstruction level. The scattering angle  $\theta$  is defined as the angle between the momentum of  $e^+$  beam and that of the  $t$  or  $\bar{t}$ . The distributions for the top and for the anti-top are related by  $\theta \rightarrow \pi - \theta$  and this is illustrated by comparing the first two plots in Figure 7. Furthermore, this holds even for the reconstructed top and anti-top candidates from the background due to CP symmetry. For this reason we consider the observable  $c = Q_l \times \cos\theta$ , i.e. the lepton charge times the cosine of the scattering angle. The discrimination power of this observable is illustrated in the right plot of Figure 7, at the reconstruction level. We perform a template fit by further dividing the signal region into 4 bins, defined as  $c \in (-1, -0.5)$ ,  $[-0.5, 0)$ ,  $[0, 0.5)$ , and  $[0.5, 1)$ . To construct a  $\chi^2$  fit, we take the  $\sqrt{B}$  in each bin as the experimental uncertainty. The smallest number of events in one bin is 24, even after requiring a  $c$ -jet, and so the Gaussian distribution is a good approximation. We simulate the Gaussian fluctuation in all bins by generating a large number of pseudo-measurements samples and computing the average  $\chi^2$  for each point in the space of coefficients. Our 95% CL bound is determined by  $\langle \chi^2 \rangle < 9.49$ .

There are two major improvements from the template fit method. First, if the SM is assumed, the 95% CL limits on the operator coefficients for  $a = 2$  are improved. This is mostly due to the  $c$ -tagging requirement. Results are shown in Figure 4 the red columns, and Figure 5 the yellow region, where the improvements are seen clearly. The same effects on the other four-fermion operators are displayed and compared in Figure 8. The second improvement is from the discrimination power

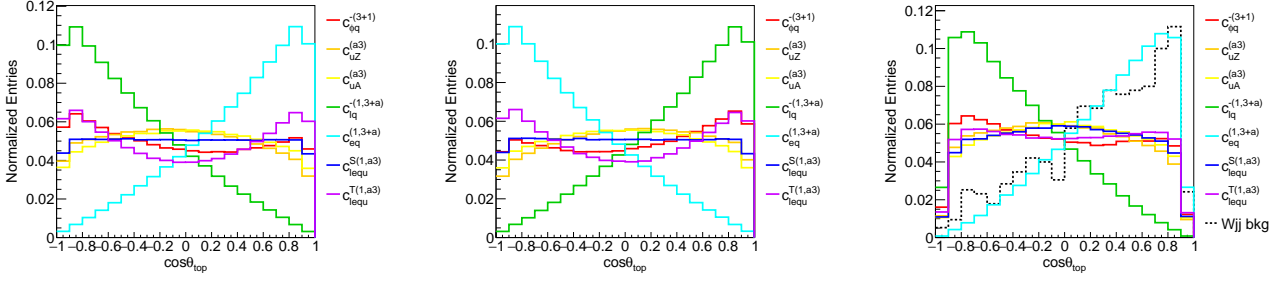


Fig. 7. Scattering angle from the seven signals of coefficients in the first row of Eq. (27).  $\theta_{top}$  is defined as the angle between the momenta of  $e^+$  beam and that of the  $t$  or  $\bar{t}$ . Left: parton level, for top production. Middle: parton level, for anti-top production. Right: reconstruction level, for top production, including the background.

between different kinds of signals, which comes from the both the angular distribution and the  $c$ -tagging information. This is particularly important when an excess is found, in which case we need to understand the FCN operator that leads to this excess. The baseline approach could only tell us the overall magnitude of the flavor-changing effects, while the template fit will help to pin down the actual form of the operator. This is illustrated in Figures 9, where we consider two hypothetical scenarios, with  $c_{eq}^{(1,3+a)} = c_{lq}^{-(1,3+a)} = 0.05$ , and  $c_{lequ}^{S(1,a3)} = 0.065$ ,  $c_{lequ}^{T(1,a3)} = 0.025$ , respectively ( $\Lambda = 1$  TeV). These values are consistent with the current bounds, but are around the sensitivity expected at the CEPC. Assuming that other coefficients vanish, with the baseline approach we would be able to identify the overall size of the flavor-changing effect, but not the individual size of each coefficient. The allowed region in the two-dimensional parameter space is a ring, giving no information to the actual form of new physics. The template fit, on the other hand, could pinpoint with more precision the value of each coefficient. This holds also for the  $a=1$  case, even though the precision is slightly worse. A four-fold degeneracy shows up in the first scenario. This is because an overall sign on all coefficients do not have a visible effect (due to absence of SM interference), and a relative sign between  $c_{eq}^{(1,3+a)}$  and  $c_{lq}^{-(1,3+a)}$  cannot be observed because the two operators do not interfere. In the second case this is reduced to a two-fold degeneracy. This is because the interference between  $c_{lequ}^{S(1,a3)}$  and  $c_{lequ}^{T(1,a3)}$  is proportional to  $\cos\theta$ , so the opposite sign case can be excluded by the angular distribution. In fact, due to the shape of the background (see Figure 7 right), the template fit has a better discrimination power when  $c_{lequ}^{S(1,a3)}$  and  $c_{lequ}^{T(1,a3)}$  take opposite signs. This effect can be seen even with the SM hypothesis, see the right plot in Figure 8. Discrimination between  $a=1$  and  $a=2$  operators are also possible with the help of  $c$ -tagging. This is demonstrated in Figure 10, where we consider three hypothetical scenarios, with  $(c_{lq}^{-(1,3+1)}, c_{lq}^{-(1,3+2)}) = (0, 0.05)$ ,  $(0.05, 0)$ , and  $(0.35, 0.35)$ . By using events with and without a  $c$ -jet,

we can resolve the light-quark flavor involved in the FCN coupling with some precision. This is unlike the LHC case, where one has to combine both production and decay measurements to disentangle the two light-quark flavors in the flavor-changing signal, by using the fact that production channel would depend on the light-quark parton distribution function.

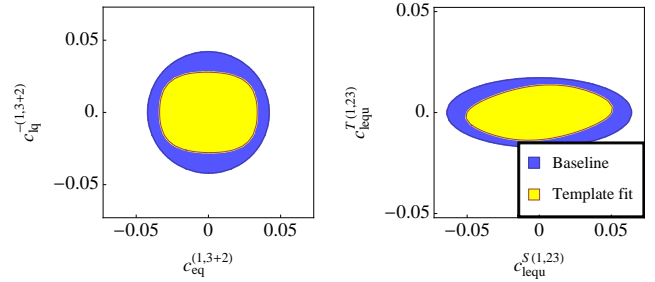


Fig. 8. Two-dimensional limits on four-fermion coefficients, at 95% CL, under the SM hypothesis, with other coefficients turned off. The template fit approach improves the sensitivity.

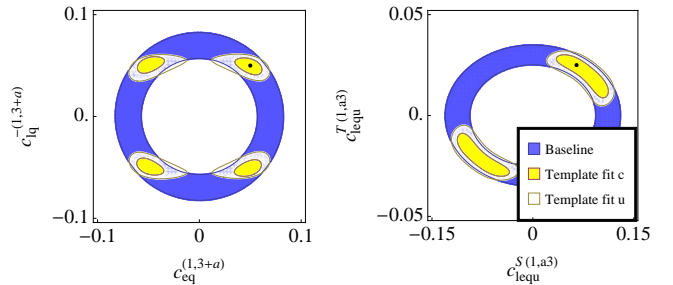


Fig. 9. Two-dimensional limits on four-fermion coefficients, at 95% CL, with other coefficients turned off. Two hypotheses are considered. Left:  $c_{eq}^{(1,3+a)} = c_{lq}^{-(1,3+a)} = 0.05$ . Right:  $c_{lequ}^{S(1,a3)} = 0.065$ ,  $c_{lequ}^{T(1,a3)} = 0.025$ . Both points are labeled by a black dot in the plots. The template fit helps to pinpoint the coefficients. Better precision is obtained for operators involving a charm-quark (i.e.  $a=2$ ).

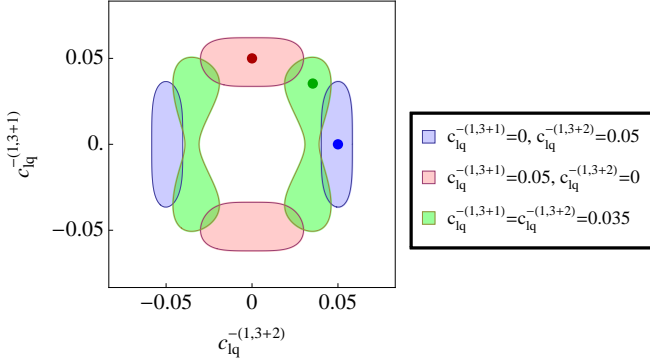


Fig. 10. Two-dimensional limits on  $c_{lq}^{-(1,3+a)}$  coefficients with  $a=1$  and  $a=2$ , at 95% CL. Other coefficients are turned off. Three hypotheses are considered. The template fit helps to identify the light-quark flavor involved in the FCN coupling.

As an additional comment, we note that a flat direction exists between the three coefficients  $c_{\varphi q}^{-(3+a)}$ ,  $c_{lq}^{-(1,3+a)}$  and  $c_{eq}^{(1,3+a)}$ , which cannot be constrained by a single run at 240 GeV. A second working point with larger energy would be useful to lift the degeneracy, as the two-fermion and four-fermion contributions depend differently on energy. All other directions can be constrained simultaneously at 240 GeV.

A more comprehensive study can further improve these results on several aspects. The QCD correction on the four-fermion operators can be implemented in the analysis, though we expect the size of the correction to be similar to the two-fermion ones. Kinematic features of the signals from different operators can be fully exploited by using a multivariate analysis. Alternatively, one could also construct the covariant matrix directly, following the statistically optimal observable [91, 92], which guarantees the best sensitivity in theory. The nonlinear form of the cross section in the parameter space and the non-analytic nature of the detector effects however need to be carefully dealt with.\* Finally, useful information may also come from the study of flavor changing decay of the top quark, depending on the possibility of an energy upgrade above the 350 GeV threshold, which in addition could also provide access to Higgs and gluon FCN couplings. We defer these studies to a future work.

## 5 Conclusion

The CEPC collider proposed as a Higgs factory is also an ideal place to study the flavor properties of the top quark. The FCN interactions of the top quark can be searched in the single top production,  $e^+e^- \rightarrow tj$ . Existing results from LEP2, Tevatron and LHC experiments suggest that a future lepton collider will provide

the best sensitivity on four-fermion FCN interactions, complementary to a hadron collider which mainly constrains two-fermion FCN interactions. In this work, we derive the expected sensitivity at the CEPC with 240 GeV energy and  $5.6 \text{ ab}^{-1}$  integrated luminosity, on the full set of 56 FCN operators that are relevant in the single top channel, and show that improvement of about 1~2 orders of magnitude on the size of four-fermion FCN couplings can be expected. Our main result is displayed in Figures 4 and 5, where one can see clearly that a large fraction of currently allowed FCN parameters can be tested by the CEPC. We also show that the capability of  $c$ -jet tagging at the CEPC further improves the sensitivity on flavor-changing couplings between the top and the charm. In case a signature is established, we show that kinematic observables can be used to pinpoint the values of the coefficients, which in turn give us information about the new physics behind the discovery.

## Acknowledgements

We would like to thank B. Fuks, G. Durieux, Z. Liang and H.-S. Shao for helpful discussions and suggestions. CZ is supported in part by CNRS via the LIA FCPPL, by the CEPC theory study grant, and by IHEP under Contract No. Y7515540U1.

## A Additional results

Here we list some additional results mentioned in the previous sections. In Figures 11 and 12, we compare the signals from  $c_{uZ}^{(a3)}$ ,  $c_{uZ}^{(3a)}$ ,  $c_{uZ}^{I(a3)}$ , and those from  $c_{eq}^{(1,3+a)}$ ,  $c_{eu}^{(1,3+a)}$ ,  $c_{eq}^{I(1,3+a)}$ . This is to illustrate the relations between coefficients in different rows of Eq. (27). In Figure 13, we show the individual limits and prospects for coefficients from the second row of Eq. (27), similar to Figure 4. In Figure 14, we present the two-dimensional bound on the two-fermion coefficient  $c_{\varphi u}^{-(3+2)}$  and the four-fermion coefficient  $c_{eu}^{(1,3+2)}$ , similar to Figure 5. Finally, in Figure 15, we show the discovery limits for coefficients of the second row of Eq. (27), similar to Figure 15.

\*The same approach has been used to study the FCN couplings at the CLIC [58], where the detector effects were taken into account by an efficiency parameter.

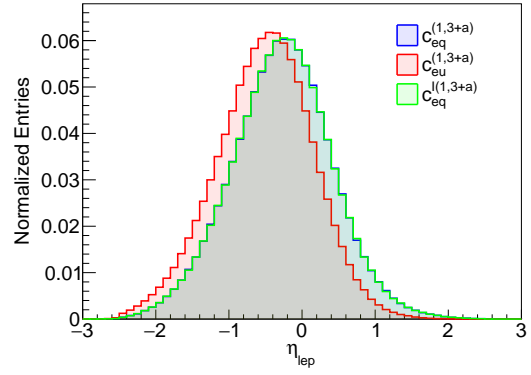
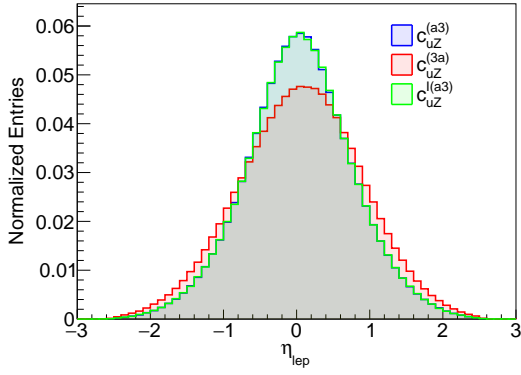
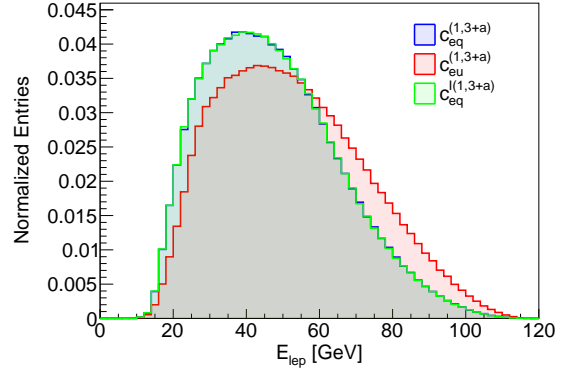
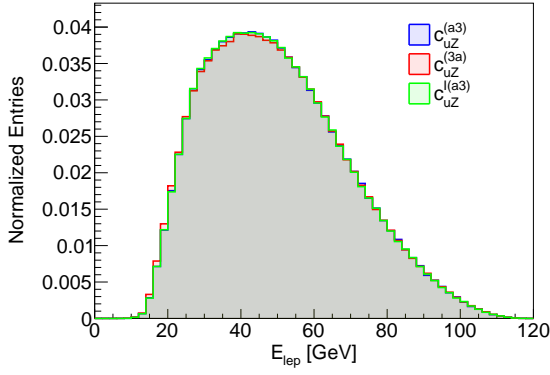
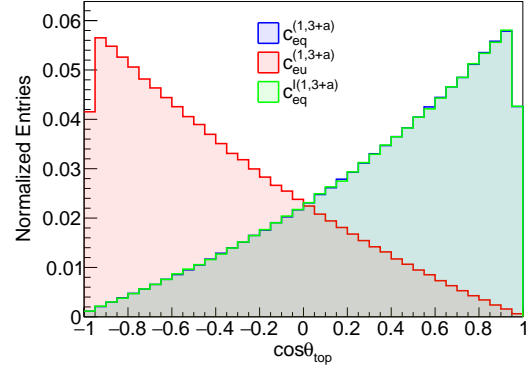
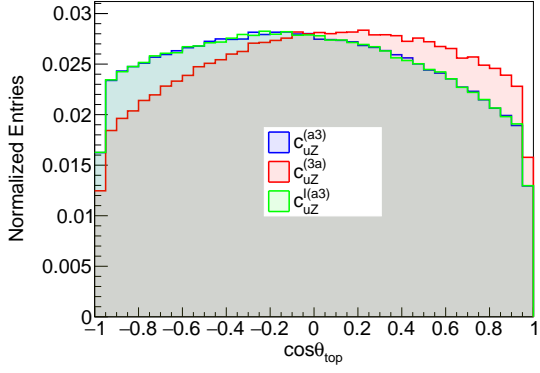


Fig. 11. Signals from  $c_{uZ}^{(a3)}$ ,  $c_{uZ}^{(3a)}$  and  $c_{uZ}^{I(a3)}$  at the parton level. Distributions of the scattering angle, the lepton energy, and the lepton pseudorapidity are compared.

Fig. 12. Signals from  $c_{eq}^{(1,3+a)}$ ,  $c_{eu}^{(1,3+a)}$  and  $c_{eq}^{I(1,3+a)}$  at the parton level. Distributions of the scattering angle, the lepton energy, and the lepton pseudorapidity are compared.

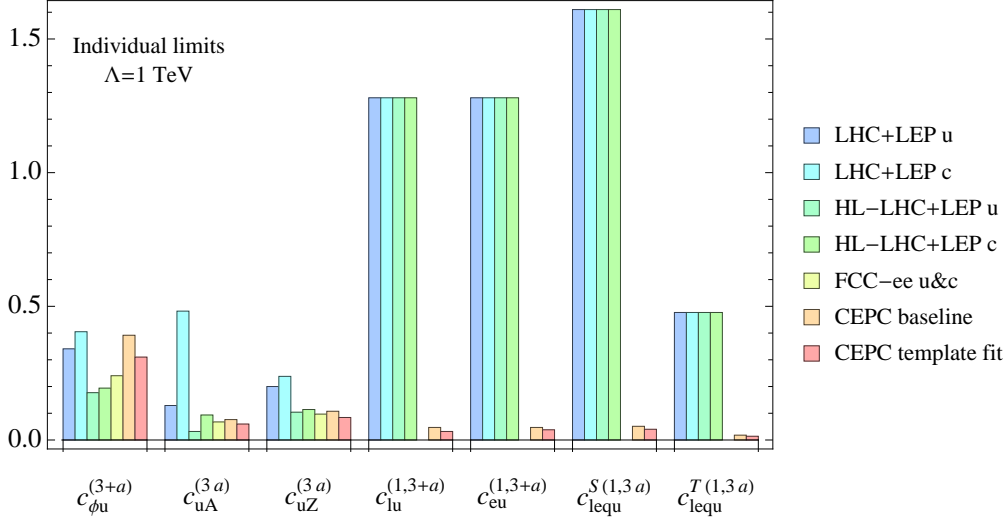


Fig. 13. The 95% CL limits on individual coefficients in the second row of Eq. (27), expected from the CEPC, compared with the existing LHC+LEP2 bounds, and the projected limits from HL-LHC+LEP2 and from FCC-ee with  $3 \text{ ab}^{-1}$  luminosity at 240 GeV (only for the first three coefficients), see Refs. [55, 57]. Results for both generations  $a = 1, 2$  are displayed. The orange column “CEPC baseline” is the expected limits following our baseline analysis, which applies to both flavors ( $a=1,2$ ). The red column “CEPC template fit” uses the  $c$ -jet tagging in its signal definition and only applies to  $a = 2$  operators.

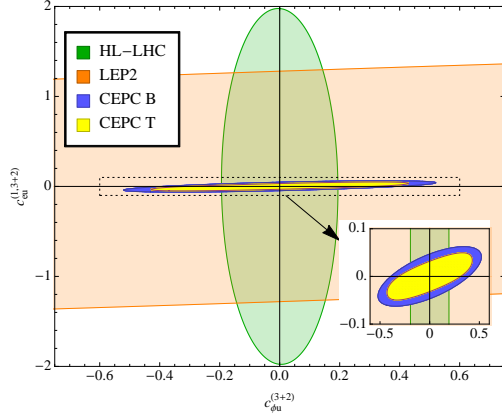


Fig. 14. Two-dimensional bounds on a two-fermion coefficient  $c_{\phi u}^{-(3+2)}$  and a four-fermion coefficient  $c_{\phi u}^{(1,3+2)}$ , at the 95% CL. Other operators are fixed at 0. The allowed regions from HL-LHC and LEP2 are similar to Figure 59 in Section 8.1 of Ref. [55], except for that there all coefficients are marginalized over. The blue region (“CEPC B”) is the bound expected from the CEPC, following our baseline analysis. The yellow region (“CEPC T”) is obtained with a template fit approach, see more discussions in Section 4.

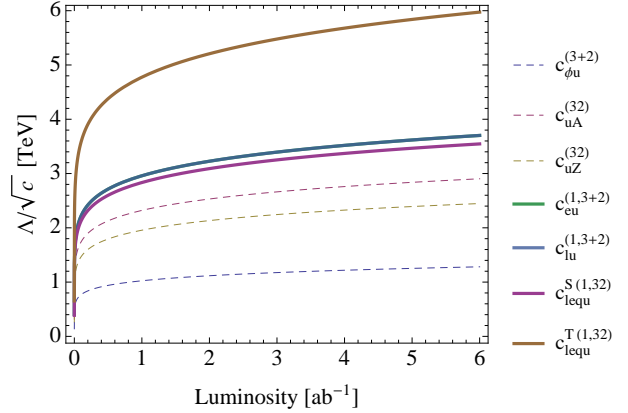


Fig. 15. Five-sigma discovery limit of  $\Lambda/\sqrt{c}$ , which is roughly the scale of new physics, for coefficients in the second row of Eq. (27), as function of integrated luminosity at the CEPC.

## References

- 1 G. Aad *et al.* [ATLAS Collaboration], Phys. Lett. B **716**, 1 (2012) doi:10.1016/j.physletb.2012.08.020 [arXiv:1207.7214 [hep-ex]].
- 2 S. Chatrchyan *et al.* [CMS Collaboration], Phys. Lett. B **716**, 30 (2012) doi:10.1016/j.physletb.2012.08.021 [arXiv:1207.7235 [hep-ex]].
- 3 M. Ahmad *et al.*, IHEP-CEPC-DR-2015-01, IHEP-TH-2015-01, IHEP-EP-2015-01.
- 4 J. Guimaraes da Costa *et al.* [CEPC Study Group], arXiv:1811.10545 [hep-ex].

- 5 E. Vryonidou and C. Zhang, JHEP **1808**, 036 (2018) doi:10.1007/JHEP08(2018)036 [arXiv:1804.09766 [hep-ph]].
- 6 S. Boselli, R. Hunter and A. Mitov, arXiv:1805.12027 [hep-ph].
- 7 G. Durieux, J. Gu, E. Vryonidou and C. Zhang, Chin. Phys. C **42**, no. 12, 123107 (2018) doi:10.1088/1674-1137/42/12/123107 [arXiv:1809.03520 [hep-ph]].
- 8 S. L. Glashow, J. Iliopoulos and L. Maiani, Phys. Rev. D **2**, 1285 (1970). doi:10.1103/PhysRevD.2.1285
- 9 F. Abe *et al.* [CDF Collaboration], Phys. Rev. Lett. **80**, 2525 (1998). doi:10.1103/PhysRevLett.80.2525
- 10 T. Aaltonen *et al.* [CDF Collaboration], Phys. Rev. Lett. **101**, 192002 (2008) doi:10.1103/PhysRevLett.101.192002 [arXiv:0805.2109 [hep-ex]].
- 11 T. Aaltonen *et al.* [CDF Collaboration], Phys. Rev. D **80**, 052001 (2009) doi:10.1103/PhysRevD.80.052001 [arXiv:0905.0277 [hep-ex]].
- 12 V. M. Abazov *et al.* [D0 Collaboration], Phys. Lett. B **701**, 313 (2011) doi:10.1016/j.physletb.2011.06.014 [arXiv:1103.4574 [hep-ex]].
- 13 M. Aaboud *et al.* [ATLAS Collaboration], JHEP **1807**, 176 (2018) doi:10.1007/JHEP07(2018)176 [arXiv:1803.09923 [hep-ex]].
- 14 G. Aad *et al.* [ATLAS Collaboration], Eur. Phys. J. C **76**, no. 1, 12 (2016) doi:10.1140/epjc/s10052-015-3851-5 [arXiv:1508.05796 [hep-ex]].
- 15 G. Aad *et al.* [ATLAS Collaboration], JHEP **1209**, 139 (2012) doi:10.1007/JHEP09(2012)139 [arXiv:1206.0257 [hep-ex]].
- 16 [ATLAS Collaboration], ATLAS-CONF-2011-154.
- 17 [ATLAS Collaboration], ATLAS-CONF-2011-061.
- 18 CMS Collaboration [CMS Collaboration], CMS-PAS-TOP-17-017.
- 19 S. Chatrchyan *et al.* [CMS Collaboration], Phys. Rev. Lett. **112**, no. 17, 171802 (2014) doi:10.1103/PhysRevLett.112.171802 [arXiv:1312.4194 [hep-ex]].
- 20 S. Chatrchyan *et al.* [CMS Collaboration], Phys. Lett. B **718**, 1252 (2013) doi:10.1016/j.physletb.2012.12.045 [arXiv:1208.0957 [hep-ex]].
- 21 M. Aaboud *et al.* [ATLAS Collaboration], [arXiv:1812.11568 [hep-ex]].
- 22 M. Aaboud *et al.* [ATLAS Collaboration], Phys. Rev. D **98**, no. 3, 032002 (2018) doi:10.1103/PhysRevD.98.032002 [arXiv:1805.03483 [hep-ex]].
- 23 A. M. Sirunyan *et al.* [CMS Collaboration], JHEP **1806**, 102 (2018) doi:10.1007/JHEP06(2018)102 [arXiv:1712.02399 [hep-ex]].
- 24 M. Aaboud *et al.* [ATLAS Collaboration], JHEP **1710**, 129 (2017) doi:10.1007/JHEP10(2017)129 [arXiv:1707.01404 [hep-ex]].
- 25 V. Khachatryan *et al.* [CMS Collaboration], JHEP **1702**, 079 (2017) doi:10.1007/JHEP02(2017)079 [arXiv:1610.04857 [hep-ex]].
- 26 G. Aad *et al.* [ATLAS Collaboration], JHEP **1512**, 061 (2015) doi:10.1007/JHEP12(2015)061 [arXiv:1509.06047 [hep-ex]].
- 27 CMS Collaboration [CMS Collaboration], CMS-PAS-TOP-14-020.
- 28 G. Aad *et al.* [ATLAS Collaboration], JHEP **1406**, 008 (2014) doi:10.1007/JHEP06(2014)008 [arXiv:1403.6293 [hep-ex]].
- 29 CMS Collaboration [CMS Collaboration], CMS-PAS-HIG-13-034.
- 30 The ATLAS collaboration [ATLAS Collaboration], ATLAS-CONF-2013-081.
- 31 T. Aaltonen *et al.* [CDF Collaboration], Phys. Rev. Lett. **102**, 151801 (2009) doi:10.1103/PhysRevLett.102.151801 [arXiv:0812.3400 [hep-ex]].
- 32 G. Aad *et al.* [ATLAS Collaboration], Eur. Phys. J. C **76**, no. 2, 55 (2016) doi:10.1140/epjc/s10052-016-3876-4 [arXiv:1509.00294 [hep-ex]].
- 33 The ATLAS collaboration [ATLAS Collaboration], ATLAS-CONF-2013-063.
- 34 G. Aad *et al.* [ATLAS Collaboration], Phys. Lett. B **712**, 351 (2012) doi:10.1016/j.physletb.2012.05.022 [arXiv:1203.0529 [hep-ex]].
- 35 V. M. Abazov *et al.* [D0 Collaboration], Phys. Lett. B **693**, 81 (2010) doi:10.1016/j.physletb.2010.08.011 [arXiv:1006.3575 [hep-ex]].
- 36 V. M. Abazov *et al.* [D0 Collaboration], Phys. Rev. Lett. **99**, 191802 (2007) doi:10.1103/PhysRevLett.99.191802 [hep-ex/0702005 [HEP-EX], arXiv:0801.2556 [HEP-EX]].
- 37 V. Khachatryan *et al.* [CMS Collaboration], JHEP **1702**, 028 (2017) doi:10.1007/JHEP02(2017)028 [arXiv:1610.03545 [hep-ex]].
- 38 V. Khachatryan *et al.* [CMS Collaboration], JHEP **1604**, 035 (2016) doi:10.1007/JHEP04(2016)035 [arXiv:1511.03951 [hep-ex]].
- 39 A. M. Sirunyan *et al.* [CMS Collaboration], JHEP **1707**, 003 (2017) doi:10.1007/JHEP07(2017)003 [arXiv:1702.01404 [hep-ex]].
- 40 D. Aleph, L3, Opal Collaborations, and the LEP Exotica Working Group, DELPHI-2001-119 CONF 542.
- 41 G. Abbiendi *et al.* [OPAL Collaboration], Phys. Lett. B **521**, 181 (2001) doi:10.1016/S0370-2693(01)01195-9 [hep-ex/0110009].
- 42 A. Heister *et al.* [ALEPH Collaboration], Phys. Lett. B **543**, 173 (2002) doi:10.1016/S0370-2693(02)02307-9 [hep-ex/0206070].
- 43 P. Achard *et al.* [L3 Collaboration], Phys. Lett. B **549**, 290 (2002) doi:10.1016/S0370-2693(02)02933-7 [hep-ex/0210041].
- 44 J. Abdallah *et al.* [DELPHI Collaboration], Phys. Lett. B **590**, 21 (2004) doi:10.1016/j.physletb.2004.03.051 [hep-ex/0404014].
- 45 J. Abdallah *et al.* [DELPHI Collaboration], Eur. Phys. J. C **71**, 1555 (2011) doi:10.1140/epjc/s10052-011-1555-z [arXiv:1102.4455 [hep-ex]].
- 46 H. Abramowicz *et al.* [ZEUS Collaboration], Phys. Lett. B **708**, 27 (2012) doi:10.1016/j.physletb.2012.01.025 [arXiv:1111.3901 [hep-ex]].
- 47 S. Chekanov *et al.* [ZEUS Collaboration], Phys. Lett. B **559**, 153 (2003) doi:10.1016/S0370-2693(03)00333-2 [hep-ex/0302010].
- 48 H1 Collaboration, "Search for single top production in  $e^{\pm}p$  collisions at HERA," H1prelim-01-063 (2001).
- 49 F. D. Aaron *et al.* [H1 Collaboration], Phys. Lett. B **678**, 450 (2009) doi:10.1016/j.physletb.2009.06.057 [arXiv:0904.3876 [hep-ex]].
- 50 A. Aktas *et al.* [H1 Collaboration], Eur. Phys. J. C **33**, 9 (2004) doi:10.1140/epjc/s2003-01588-2 [hep-ex/0310032].
- 51 G. Durieux, F. Maltoni and C. Zhang, Phys. Rev. D **91**, no. 7, 074017 (2015) doi:10.1103/PhysRevD.91.074017 [arXiv:1412.7166 [hep-ph]].
- 52 E. O. Iltan and I. Turan, Phys. Rev. D **67**, 015004 (2003) doi:10.1103/PhysRevD.67.015004 [hep-ph/0207087].
- 53 M. Frank and I. Turan, Phys. Rev. D **74**, 073014 (2006) doi:10.1103/PhysRevD.74.073014 [hep-ph/0609069].
- 54 J. Han, B. Li and X. Wang, Phys. Rev. D **83**, 034032 (2011) doi:10.1103/PhysRevD.83.034032 [arXiv:1102.4402 [hep-ph]].
- 55 A. Cerri *et al.*, arXiv:1812.07638 [hep-ph].
- 56 J. A. Aguilar-Saavedra and T. Riemann, hep-ph/0102197.
- 57 H. Khanpour, S. Khatibi, M. Khatiri Yanehsari and M. Mohammadi Najafabadi, Phys. Lett. B **775**, 25 (2017) doi:10.1016/j.physletb.2017.10.047 [arXiv:1408.2090 [hep-ph]].
- 58 J. de Blas *et al.*, CERN Yellow Rep. Monogr. Vol. 3 (2018) doi:10.23731/CYRM-2018-003 [arXiv:1812.02093 [hep-ph]].
- 59 G. Eilam, J. L. Hewett and A. Soni, Phys. Rev. D **44**, 1473 (1991) Erratum: [Phys. Rev. D **59**, 039901 (1999)]. doi:10.1103/PhysRevD.44.1473, 10.1103/PhysRevD.59.039901
- 60 B. Mele, S. Petrarca and A. Soddu, Phys. Lett. B **435**, 401 (1998) doi:10.1016/S0370-2693(98)00822-3 [hep-ph/9805498].

- 61 J. A. Aguilar-Saavedra and B. M. Nobre, Phys. Lett. B **553**, 251 (2003) doi:10.1016/S0370-2693(02)03230-6 [hep-ph/0210360].
- 62 J. A. Aguilar-Saavedra, Acta Phys. Polon. B **35**, 2695 (2004) [hep-ph/0409342].
- 63 S. Weinberg, Physica A **96**, no. 1-2, 327 (1979). doi:10.1016/0378-4371(79)90223-1
- 64 C. N. Leung, S. T. Love and S. Rao, Z. Phys. C **31**, 433 (1986). doi:10.1007/BF01588041
- 65 W. Buchmuller and D. Wyler, Nucl. Phys. B **268**, 621 (1986). doi:10.1016/0550-3213(86)90262-2
- 66 J. A. Aguilar-Saavedra *et al.*, arXiv:1802.07237 [hep-ph].
- 67 B. Grzadkowski, M. Iskrzynski, M. Misiak and J. Rosiek, JHEP **1010**, 085 (2010) doi:10.1007/JHEP10(2010)085 [arXiv:1008.4884 [hep-ph]].
- 68 S. Bar-Shalom and J. Wudka, Phys. Rev. D **60**, 094016 (1999) doi:10.1103/PhysRevD.60.094016 [hep-ph/9905407].
- 69 M. Chala, J. Santiago and M. Spannowsky, JHEP **1904**, 014 (2019) doi:10.1007/JHEP04(2019)014 [arXiv:1809.09624 [hep-ph]].
- 70 S. Davidson, M. L. Mangano, S. Perries and V. Sordini, Eur. Phys. J. C **75**, no. 9, 450 (2015) doi:10.1140/epjc/s10052-015-3649-5 [arXiv:1507.07163 [hep-ph]].
- 71 The ATLAS collaboration [ATLAS Collaboration], ATLAS-CONF-2018-044.
- 72 J. Alwall *et al.*, JHEP **1407**, 079 (2014) doi:10.1007/JHEP07(2014)079 [arXiv:1405.0301 [hep-ph]].
- 73 T. Sjostrand, S. Mrenna and P. Z. Skands, JHEP **0605**, 026 (2006) doi:10.1088/1126-6708/2006/05/026 [hep-ph/0603175].
- 74 T. Sjostrand, S. Mrenna and P. Z. Skands, Comput. Phys. Commun. **178**, 852 (2008) doi:10.1016/j.cpc.2008.01.036 [arXiv:0710.3820 [hep-ph]].
- 75 A. Alloul, N. D. Christensen, C. Degrande, C. Duhr and B. Fuks, Comput. Phys. Commun. **185**, 2250 (2014) doi:10.1016/j.cpc.2014.04.012 [arXiv:1310.1921 [hep-ph]].
- 76 C. Degrande, C. Duhr, B. Fuks, D. Grellscheid, O. Matellaer and T. Reiter, Comput. Phys. Commun. **183**, 1201 (2012) doi:10.1016/j.cpc.2012.01.022 [arXiv:1108.2040 [hep-ph]].
- 77 J. de Favereau *et al.* [DELPHES 3 Collaboration], JHEP **1402**, 057 (2014) doi:10.1007/JHEP02(2014)057 [arXiv:1307.6346 [hep-ex]].
- 78 M. Cacciari, G. P. Salam and G. Soyez, Eur. Phys. J. C **72**, 1896 (2012) doi:10.1140/epjc/s10052-012-1896-2 [arXiv:1111.6097 [hep-ph]].
- 79 M. Cacciari, G. P. Salam and G. Soyez, JHEP **0804**, 063 (2008) doi:10.1088/1126-6708/2008/04/063 [arXiv:0802.1189 [hep-ph]].
- 80 C. Degrande, F. Maltoni, J. Wang and C. Zhang, Phys. Rev. D **91**, 034024 (2015) doi:10.1103/PhysRevD.91.034024 [arXiv:1412.5594 [hep-ph]].
- 81 J. J. Liu, C. S. Li, L. L. Yang and L. G. Jin, Phys. Rev. D **72**, 074018 (2005) doi:10.1103/PhysRevD.72.074018 [hep-ph/0508016].
- 82 J. Gao, C. S. Li, J. J. Zhang and H. X. Zhu, Phys. Rev. D **80**, 114017 (2009) doi:10.1103/PhysRevD.80.114017 [arXiv:0910.4349 [hep-ph]].
- 83 Y. Zhang, B. H. Li, C. S. Li, J. Gao and H. X. Zhu, Phys. Rev. D **83**, 094003 (2011) doi:10.1103/PhysRevD.83.094003 [arXiv:1101.5346 [hep-ph]].
- 84 B. H. Li, Y. Zhang, C. S. Li, J. Gao and H. X. Zhu, Phys. Rev. D **83**, 114049 (2011) doi:10.1103/PhysRevD.83.114049 [arXiv:1103.5122 [hep-ph]].
- 85 Y. Wang, F. P. Huang, C. S. Li, B. H. Li, D. Y. Shao and J. Wang, Phys. Rev. D **86**, 094014 (2012) doi:10.1103/PhysRevD.86.094014 [arXiv:1208.2902 [hep-ph]].
- 86 J. Drobnak, S. Fajfer and J. F. Kamenik, Phys. Rev. Lett. **104**, 252001 (2010) doi:10.1103/PhysRevLett.104.252001 [arXiv:1004.0620 [hep-ph]].
- 87 J. Drobnak, S. Fajfer and J. F. Kamenik, Phys. Rev. D **82**, 073016 (2010) doi:10.1103/PhysRevD.82.073016 [arXiv:1007.2551 [hep-ph]].
- 88 C. Zhang and F. Maltoni, Phys. Rev. D **88**, 054005 (2013) doi:10.1103/PhysRevD.88.054005 [arXiv:1305.7386 [hep-ph]].
- 89 C. Zhang, Phys. Rev. D **90**, no. 1, 014008 (2014) doi:10.1103/PhysRevD.90.014008 [arXiv:1404.1264 [hep-ph]].
- 90 M. Ruan *et al.*, Eur. Phys. J. C **78**, no. 5, 426 (2018) doi:10.1140/epjc/s10052-018-5876-z [arXiv:1806.04879 [hep-ex]].
- 91 D. Atwood and A. Soni, Phys. Rev. D **45**, 2405 (1992). doi:10.1103/PhysRevD.45.2405
- 92 M. Diehl and O. Nachtmann, Z. Phys. C **62**, 397 (1994). doi:10.1007/BF01555899